J|A|C|S
ARTICLES
Published on Web 03/22/2002

Measurement of Long-Range Cross-Correlation Rates Using a Combination of Single- and Multiple-Quantum NMR Spectroscopy in One Experiment

Dominique Früh,[†] Elisabetta Chiarparin,[‡,||] Philippe Pelupessy,[§] and Geoffrey Bodenhausen*[,†,§]

Contribution from the Institut de Chimie Moléculaire et Biologique, Ecole Polytechnique Fédérale de Lausanne, BCH, 1015 Lausanne, Switzerland, Structural Biology and Molecular Modeling, Aventis Pharma, 13 quai Jules Guesde, 94403 Vitry-sur-Seine Cedex, France, and Département de Chimie, associé au CNRS, Ecole Normale Supérieure, 24 rue Lhomond, 75231 Paris Cedex 05, France

Received July 23, 2001. Revised Manuscript Received January 3, 2002

Abstract: A method is described to determine long-range cross-correlations between the modulations of an anisotropic chemical shift (e.g., of a C′ carbonyl carbon in a protein) and the fluctuations of a weak long-range dipolar interaction (e.g., in cross-correlation between the same C′ carbonyl and the H^N proton of the neighboring amide group). Such long-range correlations are difficult to measure because the corresponding long-range scalar couplings are so small that Redfield's secular approximation is often violated. The method, which combines features of single- and double-quantum NMR spectroscopy, allows one to cancel the effects of dominant short-range dipolar interactions (e.g., between the CSA of the amide nitrogen N and the dipolar coupling to its attached proton H^N) and is designed so that the secular approximation is rescued even if the scalar coupling between the long-range dipolar coupling partners is very small. The cross-correlation rates thus determined in ubiquitin cover a wide range because of local motions and variations of the CSA tensors.

Introduction

In the past few years, there has been much interest in cross-correlation effects for both structural and dynamic studies of macromolecules. Such effects have been used not only to determine dihedral angles in proteins,[1−3] but also to determine chemical shift anisotropy (CSA) tensors,[4−6] to characterize rotational diffusion tensors,[7,8] and to obtain information about hydrogen bond dynamics in nucleic acids.[9] Measurements of cross-correlation rates have also brought new insights into dynamic processes in proteins.[6,10−12] Cross-correlation processes can be exquisitely sensitive to local anisotropic motions. Indeed, a suitably chosen set of complementary relaxation rates can in principle lead to a full description of internal motions. It is therefore crucial to have access to a large number of cross-correlation rates to characterize dynamical and structural parameters. This quest has been one of the driving forces behind recent methodological developments. Selected cross-relaxation effects can be determined by focusing attention on the interconversion between specific terms of the density operator. So far, however, most of these methods have been limited to cases where the secular approximation holds, in Redfield's sense that there should not be any degeneracies between the relevant transitions in the single- or multiple-quantum spectra under investigation. Moreover, in some multiple quantum experiments, different interference effects may lead to *identical spectroscopic signatures* that cannot easily be sorted out, so that it may be necessary to use a set of complementary experiments to separate the relevant rates.

In this paper, we present a new method that simultaneously solves two of the problems mentioned above: (i) the violation of the secular approximation, and (ii) the similarity of the signatures of certain pairs of mechanisms. The new method may be regarded as a *hybrid* between single- and double-quantum

* To whom correspondence should be addressed. E-mail: Geoffrey.Bodenhausen@ens.fr. Phone: 0033 1 44 32 33 89. Fax: 0033 1 44 32 33 97.
[†] Ecole Polytechnique Fédérale de Lausanne.
[‡] Aventis Pharma.
[§] Ecole Normale Supérieure.
[||] Current address: Glaxo Smith Kline, Research Center, via Fleming 4, 37135 Verona, Italy.

(1) Reif, B.; Hennig, M.; Griesinger, C. *Science* **1997**, *276*, 1230−1233.
(2) Yang, D.; Kay, L. E. *J. Am. Chem. Soc.* **1998**, *120*, 9880−9887.
(3) Chiarparin, E.; Pelupessy, P.; Ghose, R.; Bodenhausen, G. *J. Am. Chem. Soc.* **1999**, *121*, 6876−6883.
(4) Ghose, R.; Huang, K.; Prestegard, J. H. *J. Magn. Reson.* **1998**, *135*, 487−499.
(5) Fushman, D.; Tjandra, N.; Cowburn, D. *J. Am. Chem. Soc.* **1998**, *120*, 10947−10952.
(6) Pang, Y.; Zuiderweg, E. R. P. *J. Am. Chem. Soc.* **2000**, *122*, 4841−4842.
(7) Kroenke, C. D.; Loria, J. P.; Lee, L. K.; Rance, M.; Palmer, A. G., III. *J. Am. Chem. Soc.* **1998**, *120*, 7905−7915.
(8) Deschamps, M.; Bodenhausen, G. *ChemPhysChem* **2001**, *8*−*9*, 539−543.
(9) Chiarparin, E.; Ruedisser, S.; Bodenhausen, G. *ChemPhysChem* **2001**, *2*, 41−45.
(10) Daragan, V. A.; Mayo, K. H. *Prog. Nucl. Magn. Reson. Spectrosc.* **1997**, *31*, 63−105.
(11) Brutscher, B.; Skrynnikov, N. R.; Bremi, T.; Brüschweiler, R.; Ernst, R. R. *J. Magn. Reson.* **1998**, *130*, 346−351.
(12) Früh, D.; Tolman, J. R.; Bodenhausen, G.; Zwahlen, C. *J. Am. Chem. Soc.* **2001**, *123*, 4810−4816.

10.1021/ja011790v CCC: $22.00

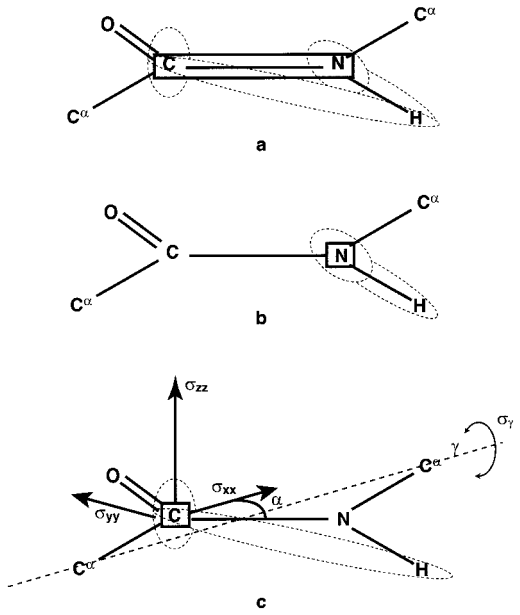

Figure 1. Two cross-correlation mechanisms may lead to the interconversion of in-phase and antiphase density operator terms $\langle B\rangle$ and $\langle 2BH_z\rangle$ in an amide group $C'ONH^N$ of a protein. (a) During multiple-quantum relaxation (where $B = 2C_yN_x$ represents a superposition of double- and zero-quantum coherences), there are two CSA/dipolar cross-correlated mechanisms, that is, the dominant N/NH^N and the long-range $C'/C'H^N$ mechanisms that contribute to cross-relaxation, that is, to the interconversion between $2C'_yN_x$ and $4C'_yN_xH_z$. (b) During single-quantum precession intervals (where $B = N_y$), only the dominant N/NH^N interference effect can lead to an interconversion between N_y and $2N_yH_z$. (c) The effect of the N/NH^N cross-correlation mechanism is averaged out by combining multiple- and single-quantum relaxation periods, so that only the long-range $C'/C'H^N$ mechanism remains effective. The principal components of the CSA tensor σ_{xx}, σ_{yy}, and σ_{zz} are oriented so that σ_{zz} is perpendicular to the peptide plane, while σ_{xx} subtends an angle α with respect to the CN bond. In the one-dimensional Gaussian amplitude fluctuation (1D-GAF) model,[37] motions through an angle σ_γ are considered around the axis γ (dashed line) defined by the two neighboring C^α carbons.

spectroscopy and can be applied to a wide variety of problems. We illustrate this general method by applications to the measurement of the cross-correlation rate $R_{C'/C'H^N}$ involving the CSA of the carbonyl carbon C′ and the long-range dipolar $C'H^N$ interaction. This rate turns out to be very sensitive both to dynamics and to structural variations of the CSA tensor.[11,13] This fact underscores the need for the measurement of complementary cross-correlation rates to separate contributions of dynamic and structural properties.

Materials and Methods

Uniformly ^{13}C and ^{15}N-enriched ubiquitin was obtained commercially (VLI). The protein was dissolved in 10% D_2O/90% H_2O at pH 4.5 to a concentration of 1.5 mM in a Shigemi tube. NMR data were acquired at 30 °C with a Bruker DMX-600 spectrometer equipped with a triple resonance TBI probe with triple axis gradients. The 2D spectra were recorded with the pulse scheme shown in Figure 2, with a relaxation delay of 1.5 s between subsequent scans; the spectral widths were 1824 and 8389 Hz in the ω_1 and ω_2 dimensions. The total measurement time for a pair of 2D spectra was 9.5 h. The data were processed using the package nmrPipe/nmrDraw.[14] Linear prediction was used to extend the data matrix from 32×512 to 64×512 complex points. Each dimension was apodized with a squared cosine-bell window function and zero-filled once. Relaxation rates were obtained by least-squares fitting of the build-up curves, by using the Levenberg−Marquardt algorithm in matlab.[15] Errors were estimated by using a Monte Carlo analysis with 300 synthetic data sets.[16]

Pulse Sequence and Methodology. Cross-correlation effects can be studied by a wide variety of methods.[17] Because these effects lead to differential line-broadening (or, as optimists will appreciate, line-narrowing), the ratios of the peak intensities of individual lines within a multiplet can provide a direct measure of cross-correlation rates.[1,18] This can be shown by expanding the density operator in a single-transition basis and by using Redfield theory for single transitions.[19] On the other hand, if one uses a basis $\{B_i\}$ of products of Cartesian angular momentum operators,[20] cross-correlation effects can be rationalized in terms of interconversions between different terms of the density operator. This situation is best described by using Redfield's double commutator formalism. The cross-correlation rate can be determined by measuring the decay of a "source" term B_I ("diagonal peak" with amplitude a(I)) and the build-up of a "destination" term B_{II} ("cross-peak" with amplitude a(II)). In both strategies, the interpretation of the rates is greatly simplified if the secular approximation is fulfilled, that is, if the cross-relaxation rate that couples the single transition operators is smaller than the difference between their precession frequencies. The time-dependence of two single-transition coherences σ_{rs} and σ_{tu} is governed by the differential equation:

$$\frac{d}{dt}\begin{pmatrix}\sigma_{rs}\\ \sigma_{tu}\end{pmatrix} = \begin{pmatrix}-i\omega_{rs} + R_{rsrs} & R_{rstu}\\ R_{rstu} & -i\omega_{tu} + R_{tutu}\end{pmatrix}\begin{pmatrix}\sigma_{rs}\\ \sigma_{tu}\end{pmatrix} \qquad (1)$$

where ω_{rs} and ω_{tu} are the precession frequencies, R_{rsrs} and R_{tutu} are the auto-relaxation rates, and R_{rstu} is the coupling term, which can be neglected provided it is smaller than the difference between the diagonal elements (this corresponds to Redfield's "secular approximation"). In the case of CSA/DD cross-correlations acting on a single-quantum coherence (e.g., C'_+) which involve a dipolar interaction (e.g., $C'-H^N$) with an external passive spin I (e.g., H^N), this off-diagonal rate (i.e., the rate that couples $C'_+H^N_\alpha$ and $C'_+H^N_\beta$) can be estimated to be half of the difference ΔR between the autorelaxation rates of coherences that are in-phase and antiphase (i.e,. C'_+ and $2C'_+H^N_z$) with respect to the external spin I. To a good approximation, this difference ΔR corresponds to the longitudinal autorelaxation rate $1/T_1(I)$ of the external spin.[21,22] In other words, the secular approximation is fulfilled if the longitudinal relaxation rate $1/T_1(I)$ of the external spin is much smaller than the *effective* scalar coupling between this external spin I and the coherence under investigation. Thus, the long-range $R_{C'/C'H^N}$ cross-correlation rate cannot be easily extracted from the line-widths of the doublet of the carbonyl C′ single-quantum coherence (SQC), since the relevant coupling constant $^2J(C'H^N)$ may be smaller than the rate $1/T_1(H^N)$, which is dominated by dipolar interactions with neighboring spins and by chemical exchange. However, a double- or zero-quantum coherence (DQC or ZQC) involving both the C′ carbon and the neighboring amide nitrogen N (i.e., C'_+N_+ or C'_-N_+) benefits from a much larger effective scalar coupling with the amide proton, $J_{eff} = {}^1J(NH^N) \pm {}^2J(C'H^N)$, thus restoring the validity of the secular approximation and allowing one to measure the long-range $C'/C'H^N$ cross-correlation effect.

It can be shown that the dominant N/NH^N cross-correlation mechanism has the same effect on the DQC and ZQC as the long-range $C'/C'H^N$ mechanism. In a Cartesian basis, both $C'/C'H^N$ and N/NH^N

(13) Pang, Y.; Wang, L.; Pellechia, M.; Kurochkin, A. V.; Zuiderweg, E. R. P. *J. Biomol. NMR* **1999**, *14*, 297−306.
(14) Delaglio, F.; Grzesiek, S.; Vuister, G. W.; Zhu, G.; Pfeifer, J.; Bax, A. *J. Biomol. NMR* **1995**, *6*, 277−293.
(15) *Matlab Reference Guide*; Math Works Inc.: Natick, MA, 1992.
(16) Bevington, P. R.; Robinson, D. K. *Data Reduction and Error Analysis for the Physical Sciences*; McGraw-Hill, Inc.: New York, 1992.
(17) Anil Kumar; Grace, R. C. R.; Madhu, P. K. *Prog. Nucl. Magn. Reson. Spectrosc.* **2000**, *37*, 191−319.
(18) Boyd, J.; Hommel, U.; Krishnan, V. V. *Chem. Phys. Lett.* **1991**, *187*, 317−324.
(19) Redfield, A. G. *Adv. Magn. Reson.* **1965**, *1*, 1−32.
(20) Sørensen, O. W.; Eich, G. W.; Levitt, M. H.; Bodenhausen, G.; Ernst, R. R. *Prog. Nucl. Magn. Reson. Spectrosc.* **1983**, *16*, 163−192.
(21) Goldman, M. *J. Magn. Reson.* **1984**, *60*, 437−452.
(22) Goldman, M. *J. Magn. Reson.* **2001**, *149*, 160−187.

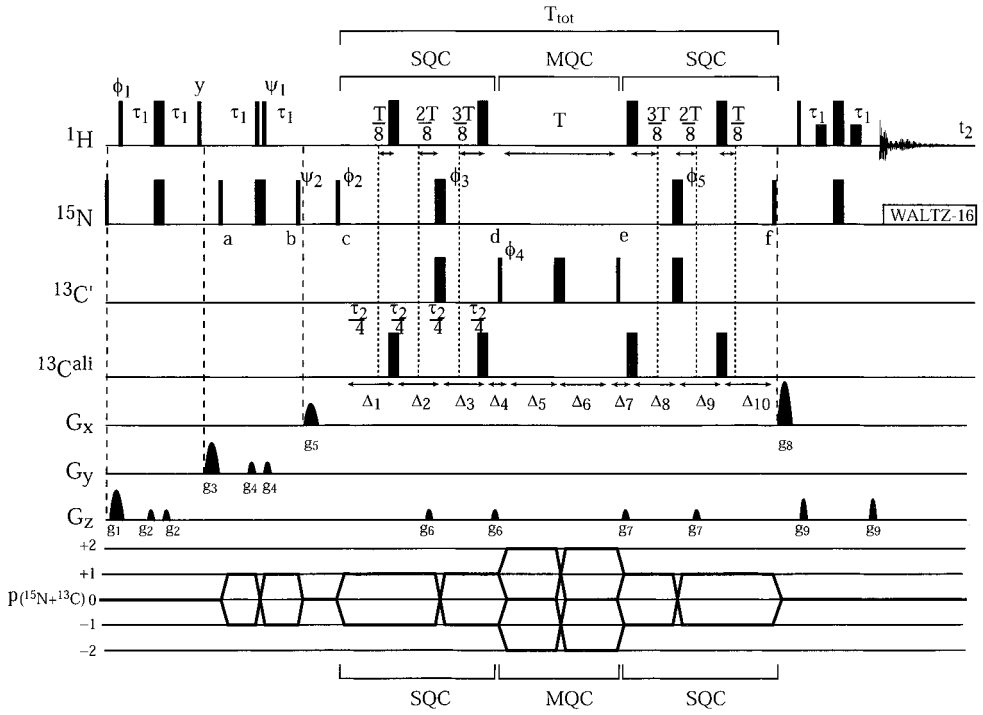

Figure 2. Pulse sequences and coherence transfer pathways of the hybrid scheme used to measure the cross-correlation rate $R_{C'/C'H^N}$. Narrow and wide rectangles indicate 90° and 180° pulses, respectively. Lower rectangles stand for selective rectangular 90° pulses applied at the water frequency. The pulses are applied along the *x*-axis unless specified otherwise. The ^{1}H, ^{15}N, and ^{13}C carriers are positioned at 4.7, 118, and 175 ppm, respectively. Two composite pulses[40] are applied to refocus the ^{15}N single quantum coherences between points **c** and **f**. Pulses applied to the aliphatic carbons are obtained by phase modulation. The carbon pulses have field strengths of $\Delta\nu/\sqrt{15}$ and $\Delta\nu/\sqrt{3}$ Hz for 90° and 180° pulses, where $\Delta\nu$ is the difference between the centers of the ^{13}C′ and the $^{13}C^{ali}$ regions ($\Delta\nu$ = 17 655 Hz at 600 MHz). The delays are set to $\tau_1 = 1/(4^1J(NH^N)) = 2.7$ ms, $\tau_2 = 1/(2^1J(C'N)) = 33$ ms, $\Delta_1 = \Delta_2 = \Delta_9 = \Delta_{10} = T_{tot}/8 - t_1/8 = \tau_2/4 + T/8 - t_1/8$, $\Delta_3 = \Delta_8 = T_{tot}/8 + t_1/8 = \tau_2/4 + T/8 + t_1/8$, $\Delta_4 = \Delta_7 = T_{tot}/8 - T/2 + t_1/8 = \tau_2/4 - 3T/8 + t_1/8$. Note that the symbols Δ_i refer to the actual delays that must be implemented by the pulse programmer, the symbols τ_i indicate their relationships with the scalar couplings, while *T* refers to the discussion of cross-correlated relaxation effects. The evolution under the ^{15}N chemical shifts in the single-quantum coherence (SQC) intervals is allowed in the manner of constant-time experiments by incrementing the delays Δ_3, Δ_4, Δ_7, and Δ_8 by $t_1/8$ while decrementing Δ_1, Δ_2, Δ_9, and Δ_{10} by the same amount. The phase of the signal is adjusted to pure absorption in the indirect ω_1 dimension by shifting the ^{15}N refocusing pulses by *T*/4 from the center of the SQC intervals. The 180° pulse applied to the ^{13}C′ carbonyl carbon during the multiple-quantum coherence (MQC) interval refocuses the C′ chemical shifts. Quadrature detection is obtained in ω_1 by the States-TPPI technique.[25] The Watergate scheme[26] inserted just before acquisition ensures effective suppression of the water resonance. Nitrogen decoupling is achieved by using WALTZ-16[41] with a radio frequency field strength of 1.2 kHz. The phase cycle is $\phi_1 = x, x, -x, -x, \phi_2 = x, -x, x, -x, \phi_3 = 8(x), 8(y), 8(-x), 8(-y), \phi_4 = 4(x), 4(-x)$. For experiment I ("source term" or "diagonal peak"), $\psi_1 = -x, \psi_2 = -x, \phi_5 = x$, and $\phi_{rec} = 2(x, -x, -x, x, -x, x, x, -x, -x, x, x, -x, x, -x, -x, x)$. For experiment II ("destination term" or "cross-peak"), $\psi_1 = x, \psi_2 = -y, \phi_5 = 32(x), 32(y), 32(-x), 32(-y)$, and $\phi_{rec} = 2(2(x, -x, -x, x, -x, x, x, -x, -x, x, x, -x, x, -x, -x, x), 2(-x, x, x, -x, x, -x, -x, x, x, -x, -x, x, -x, x, x, -x))$. The gradients g_1, g_3, g_5, and g_8 destroy unwanted coherences, while the two g_9 gradients are part of the water suppression scheme. Other gradients are applied to cancel pulse imperfections. The gradients have the following durations and strengths: g_1 = (1 ms, 46.5 G/cm), g_2 = (1 ms, 7.5 G/cm), g_3 = (1 ms, 21.25 G/cm), $g4$ = (1 ms, 2.25 G/cm), $g5$ = (1 ms, 16.75 G/cm), $g6$ = (500 μs, 9.5 G/cm), $g7$ = (500 μs, 7.5 G/cm), $g8$ = (1 ms, 22.25 G/cm), and $g9$ = (500 μs, 15.5 G/cm).

cross-correlation effects transform the density operator term $2C'_yN_x$ into $4C'_yN_xH_z$ so that the measured rate corresponds to the sum $R_{C'/C'H^N} + R_{N/NH^N}$. Although the dominant rate R_{N/NH^N} can be measured[23] by a separate ^{15}N SQC experiment (where the secular approximation holds), this procedure is not only time-consuming, as discussed at the end of this section, but also prone to subtraction errors since $R_{C'/C'H^N} \ll R_{N/NH^N}$. To isolate the effect of the long-range C′/C′H^N interaction from that of the dominant N/NH^N interference, we propose a more efficient experiment where the N/NH^N effect acting during two SQC intervals cancels the effect of the same N/NH^N interaction during an MQC interval (Figure 1). In essence, the conversion from $2C'_yN_x$ to $4C'_yN_xH_z$ during the MQC period is balanced by the conversion from $2N_yH_z$ to N_y during the SQC intervals. In doing so, the unwanted dominant rate is averaged to zeroth-order (vide infra). The long-range cross-correlation rate $R_{C'/C'H^N}$ can then simply be obtained by measuring the decay of $\langle 4C'_yN_xH_z\rangle$ ("diagonal peak", experiment I) and the build-up of $\langle 4C'_yN_xH_z\rangle$ from $\langle 2C'_yN_x\rangle$ ("cross-peak", experiment II), and by fitting the ratio of the corresponding signals with a hyperbolic tangent function:[3,23]

$$\frac{a(II)}{a(I)} = \frac{\exp(R_{C'/C'H^N}T) - \exp(-R_{C'/C'H^N}T)}{\exp(R_{C'/C'H^N}T) + \exp(-R_{C'/C'H^N}T)} = +\tanh(R_{C'/C'H^N}T) \quad (2)$$

In doing so, the relevant basis of the density operator is in effect reduced to the subset $\{2C'_yN_x,\ 4C'_yN_xH_z\}$. The pulse sequence used for measuring the cross-correlation rate $R_{C'/C'H^N}$ is shown in Figure 2. After a first INEPT sequence leading to a single-quantum coherence $-2N_yH_z$ at point **a**, an interval $2\tau_1$ is inserted to enable subsequent selection of either a(I) or a(II) signals. To measure a(I), one chooses $\psi_1 = -x$, so that the evolution under the one-bond scalar coupling $^1J(NH^N)$ is refocused at point **b**. The density operator $-2N_yH_z$ at point b is therefore the same as that at point **a**. To measure a(II), one must set $\psi_1 = x$, so that the antiphase coherence $-2N_yH_z$ at point **a** is converted into in-phase coherence N_x at point **b**. The phase ψ_2 is then adjusted to convert the selected coherence into longitudinal two-spin order $2N_zH_z$ (experiment I) or into N_z (experiment II), and a z-filter[24] is applied to destroy unwanted coherences. For sequence II, this scheme has the added benefit of suppressing coherences associated with RCONHH′ groups in the side-chains of asparagines and glutamines ($^1J(NH) \simeq {}^1J(NH')$), which have a phase that is orthogonal to that of

(23) Tjandra, N.; Szabo, A.; Bax, A. *J. Am. Chem. Soc.* **1996**, *118*, 8, 6986−6991.
(24) Sørensen, O. W.; Rance, M.; Ernst, R. R. *J. Magn. Reson.* **1984**, *56*, 527−534.

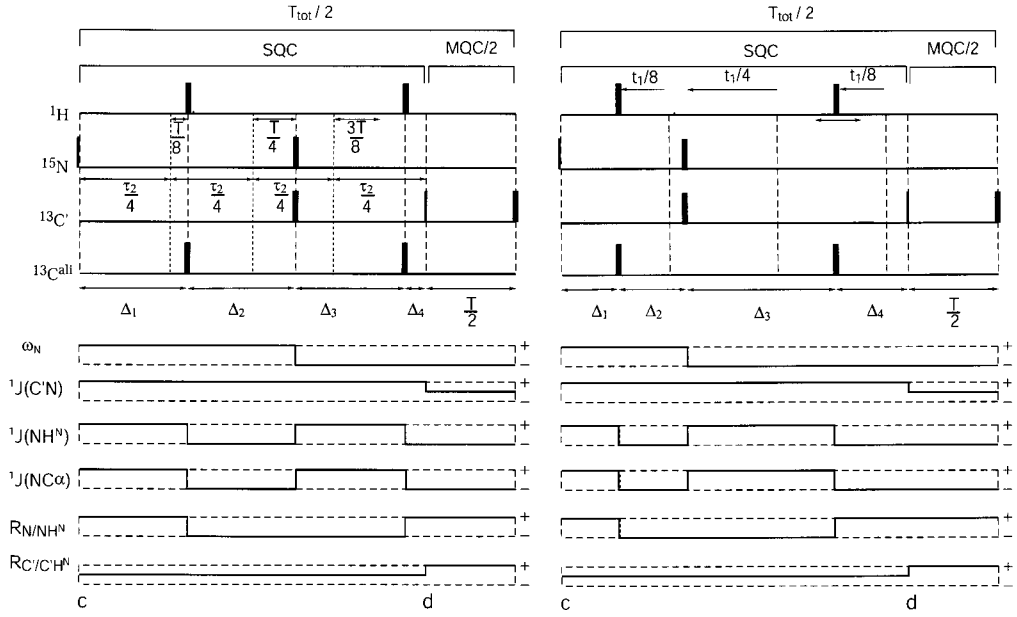

Figure 3. (Left) Averaging of coherent and incoherent processes during the SQC/MQC periods for an evolution time $t_1 = 0$. For clarity, only the first half $T_{tot}/2$ of the symmetric interval T_{tot} between points **c** and **f** in Figure 2 is shown. In the lower part, "toggling frame diagrams"[3] depict the alternation of the effective signs of various interactions (scalar couplings, chemical shifts, and cross-correlation rates). Their signs can be reversed by applying 180° pulses at suitable positions. For $t_1 = 0$, the 180° refocusing pulse applied to ^{15}N is in the center of the first half $T_{tot}/2$ of the interval T_{tot}, which ensures perfect phasing in the ω_1 dimension. The ^{1}H and $^{13}C^{ali}$ 180° pulses are positioned to cancel the evolution under the $^1J(NH^N)$ and $^1J(NC^\alpha)$ couplings and to average out the effects of the dominant cross-correlation rate R_{N/NH^N} during the interval T_{tot}. (Right) Same as on left, showing that the undesirable interactions also cancel for an arbitrary duration of the evolution time t_1. The effective evolution intervals during the whole T_{tot} period are t_1 for the ^{15}N chemical shifts, $2 \times [1/(2^1J(C'N))]$ for $^1J(C'N)$, that is, $1/(2^1J(C'N))$ to create the doubly antiphase coherence $4C'_zN_xH_z$ and $1/(2^1J(C'N))$ to restore the singly antiphase coherence $2N_yH_z$, and T for the long-range cross-correlation rate $R_{C'/C'H^N}$.

the desired magnetization of backbone amide NH^N groups. Between points **a** and **b**, these coherences evolve as follows:

$$-2N_yH_z \xrightarrow{\substack{\pi J(NH)2N_zH_z2\tau_1 + \\ \pi J(NH')2N_zH'_z2\tau_1}}$$

$$-2N_yH_z \cos(\pi J(NH)2\tau_1)\cos(\pi J(NH')2\tau_1) + N_x \sin(\pi J(NH)2\tau_1)\cos(\pi J(NH')2\tau_1) + 4N_xH'_zH_z \cos(\pi J(NH)2\tau_1) \times \sin(\pi J(NH')2\tau_1) + 2N_yH'_z \sin(\pi J(NH)2\tau_1)\sin(\pi J(NH')2\tau_1) \quad (3)$$

The suppression of the last term is of prime importance, as it may lead to strong *dispersive* signals, which tend to obscure the weak signals of experiment II. From point c to d, SQC of the amide nitrogen N is allowed to evolve under the one-bond scalar coupling $^1J(C'N)$ so that one obtains the desired multiple-quantum coherence MQC term $2C'_yN_x$ (a superposition of ZQC and DQC) after a 90° pulse applied to the carbonyl carbon C′. During the relaxation interval T, the MQC is affected both by the long-range $C'/C'H^N$ cross-correlation mechanism and by the dominant N/NH^N interference. A 180° pulse applied to C′ refocuses the evolution under the C′ chemical shift and under scalar couplings between C′ and other nuclei. The magnetization is then transferred back to H^N. The ^{15}N chemical shift is allowed to evolve in a constant-time manner during the whole SQC/MQC/SQC interval T_{tot} between points **c** and **f**. Protons and aliphatic carbons are decoupled by 180° pulses during this period. The locations of these pulses have been designed to compensate evolution during the relaxation period (see below for details). Pure absorption signals are obtained in the ω_1 domain by using the States-TPPI technique.[25] Water suppression is achieved by the Watergate technique.[26] Only the density operator term $2N_yH_z$ at point **f** leads to a detectable signal for $t_1 = 0$. Because couplings to protons cannot evolve during the SQC/MQC/SQC interval T_{tot}, the signal in experiment II can only arise from the long-range C′/$C'H^N$ cross-correlation mechanism.

Figure 3 shows the first half of the symmetric SQC/MQC/SQC interval T_{tot}. The values of the delays Δ_i have been calculated to avoid simultaneously the evolution under the scalar couplings $^1J(NH^N)$ and $^1J(NC^\alpha)$ and manifestations of the N/NH^N cross-correlation mechanism during the overall period T_{tot}. The toggling frames in Figure 3 summarize the evolution of some of the interactions. All scalar couplings, chemical shifts, and cross-correlation rates, in particular of the dominant rate R_{N/NH^N}, are averaged to zero regardless of the duration of t_1, except for the nitrogen chemical shift which evolves during t_1 and the long-range cross-correlation rate $C'/C'H^N$ which is effective during the interval T. Other interference effects, such as NH^i/NH^j or NH^i/NC^α (i, j = α, β, N), only contribute to the signal a(II) via second-order processes.[3]

The toggling frame diagram of Figure 3 merely depicts a zeroth-order representation of various processes occurring during the first half of the interval T_{tot}. Because the long-range $R_{C'/C'H^N}$ rate that we wish to determine is very weak, an analysis of higher order effects is worthwhile. Differential relaxation of in-phase and antiphase coherences may lead to imperfect refocusing of couplings and unwanted cross-correlation rates.[27] Numerical simulations of the evolution of the density operator show that second-order contributions to the build-up of $\langle 4C'_yN_xH_z\rangle$ through nonsecular effects mediated by $^1J(NH^N)$ and by R_{N/NH^N} are negligible (see Supporting Information). However, additional contributions to the build-up of the detected coherence $2N_yH_z$ may occur through *longitudinal* $C'/C'H^N$ cross-correlation that may transform the term $2C'_zN_x$ into $4C'_zN_xH_z$, which is then converted into $2N_yH_z$ under the evolution of the scalar coupling $^1J(C'N)$. This contribution can only affect an SQC of spin N that is in antiphase with respect to the carbonyl carbon. Moreover, it is partially averaged out by the C′ and proton π pulses. Simulations show that this effect systematically attenuates the

(25) Marion, D.; Ikura, M.; Tschudin, R.; Bax, A. *J. Magn. Reson.* **1989**, *85*, 393−399.
(26) Piotto, M.; Saudek, V.; Sklenar, V. *J. Biomol. NMR* **1992**, *2*, 661−665.
(27) Meersmann, T.; Bodenhausen, G. *Chem. Phys. Lett.* **1996**, *257*, 374−380.

measured rate $R^{app}_{C'/C'H^N}$ by a factor of $1/(1+\epsilon)$ where $\epsilon = 0.1$ for $\tau_c = 4.1$ ns[28] at 600 MHz. Thus, the true transverse cross-correlation rate $R_{C'/C'H^N}$ can be obtained from the apparent measured rate $R^{app}_{C'/C'H^N}$:

$$R_{C'/C'H^N}(2C'_yN_x) = (1+\epsilon)R^{app}_{C'/C'H^N} \quad (4)$$

It is important to note that both longitudinal and transverse contributions arise from the same mechanism and thus depend on the same dynamical and structural parameters (see Supporting Information for more details).

It might appear that information about long-range correlations could be extracted more conveniently by recording separately an MQC and a SQC experiment, rather than a single hybrid experiment. Indeed, such a double-barrelled method would also be a novel approach, which could be particularly useful if the protons were exchanging rapidly, since one could decouple the protons during the τ_2 intervals of Figure 3. Care should of course be taken to ensure that heating effects are comparable for the separate MQC and SQC experiments. A normal MQC experiment would require a pulse sequence which is similar to the one shown in Figure 2, except that the filter between time points **a** and **b** of duration $2\tau_1 = 5.3$ ms can be removed. For ubiquitin, where nitrogen-15 single-quantum coherences have transverse relaxation times T_2 on the order of 170 ms, this would only give a marginal gain. On the other hand, a pure SQC experiment would give an improvement in S/N of nearly a factor of $^3/_2$, as compared to a pure MQC experiment, assuming that losses are only due to relaxation. The build-up rate of the dominant interaction $R_{N,NH}$ could thus be determined with an error reduced to about $^2/_3$, as compared to the hybrid experiment. Thus, if the total available time were equally split between an MQC and an SQC experiment, the relative error on the long-range cross-correlation rate $R_{C'/C'H^N}$ would actually be degraded by a factor of 1.7. A more appropriate manner of partitioning the total available time could reduce this loss, but the hybrid experiment is always more efficient. Note that even a small systematic error in the single quantum experiment might result in a large inaccuracy in the determination of the long-range rate. It should also be noted that the hybrid experiment does not merely cancel a variety of undesirable rates by arithmetic subtraction, but that these rates act with opposite signs during the two SQC and the MQC intervals in Figure 3.

Results and Discussion

Figure 4 shows typical spectra obtained with the two complementary experiments I and II described in Figure 2 with ^{13}C and ^{15}N doubly enriched human ubiquitin. Nonvanishing signals were detected for 69 pairs of amino acids (out of a total of 76 pairs). In the following, the peptide planes will be labeled by specifying first the residue containing the carbonyl carbon C′ and then the amino acid carrying the amide nitrogen N. Pairs of residues with signals that overlap were excluded from further analysis, T9/G10, V17/E18, V26/K27, I30/Q31, L71/R72, H68/L69, and R72/L73. The remaining peaks were integrated using the nmrPipe package. For both experiments I and II, the relaxation time T was incremented between 10 and 18 ms in 9 steps of 1 ms. Figure 5 shows representative build-up curves of the ratio a(II)/a(I) for a few residues located in a loop (Figure 5a), an α helix (Figure 5b), and a β strand (Figure 5c). For each ratio, the error was calculated from an estimate of the noise level in the corresponding experiments. The measured cross-correlation rates $R^{app}_{C'/C'H^N}$ were then obtained by fitting to eq 2. The errors of these cross-correlation rates were estimated by a Monte Carlo procedure with 300 synthetic data sets generated using a random Gaussian distribution.[16] The experiment was carried out twice to evaluate the reproducibility of the results (see Supporting Information.)

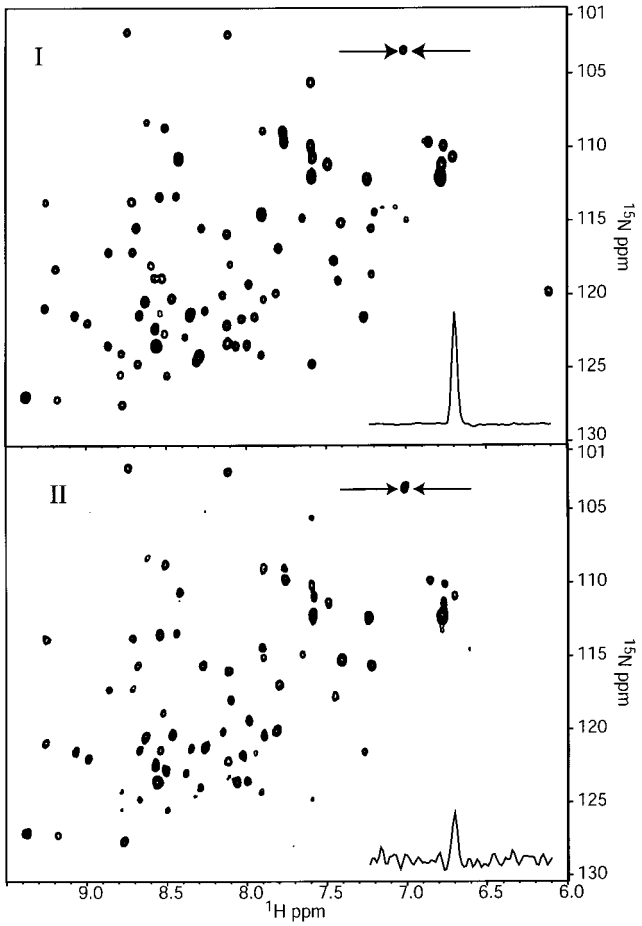

Figure 4. Correlation spectra showing the shifts of the amide ^{15}N and $^1H^N$ nuclei of doubly enriched $^{13}C/^{15}N$ ubiquitin obtained with the pulse sequences described in Figure 2, for a relaxation period $T = 17$ ms. Top: experiment I with amplitudes of "diagonal" or "source" signals. Bottom: experiment II with "cross-peak" or "destination" signals. Cross-sections parallel to the horizontal ω_2 axes at the ^{15}N shift of residue S20 (signals due to the pair of amino acids P19/S20) are shown. The acquisition times were 1 h for experiment I and 8.5 h for experiment II.

For an arbitrary CSA tensor, the rate $R_{C'/C'H^N}$ can be calculated by[21]

$$R_{C'/C'H^N} = \frac{1}{6}\hbar\frac{\gamma_C{}^2\gamma_H B_0}{r^3_{C'H^N}}\{(\sigma_{xx}-\sigma_{zz})[4J_{xx,C'H^N}(0) + 3J_{xx,C'H^N}(\omega_C)] + (\sigma_{yy}-\sigma_{zz})[4J_{yy,C'H^N}(0) + 3J_{yy,C'H^N}(\omega_C)]\} \quad (5)$$

where σ_{ii} are the principal components of the CSA tensor of Figure 1, and the other symbols have their usual meanings. $J_{ii,C'H^N}(\omega)$ are the cross-correlation spectral densities[10,29]

$$J_{ii,C'H^N}(\omega_C) = \frac{2}{5}\left[\frac{S^2_{ii,C'H^N}\tau_C}{1+(\omega_C\tau_C)^2} + \frac{(P_2(\cos\theta_{ii,C'H^N}) - S^2_{ii,C'H^N})\tau}{1+(\omega_C\tau)^2}\right] \quad (6)$$

where τ_c is the overall rotational correlation time, and τ is defined so that $\tau^{-1} = \tau_c{}^{-1} + \tau_e{}^{-1}$, with the local correlation

(28) Schneider, D. M.; Dellwo, M. J.; Wand, A. J. *Biochemistry* **1992**, *31*, 3645−3652.

(29) Brüschweiler, R.; Ernst, R. R. *J. Chem. Phys.* **1992**, *96*, 1758−1766.

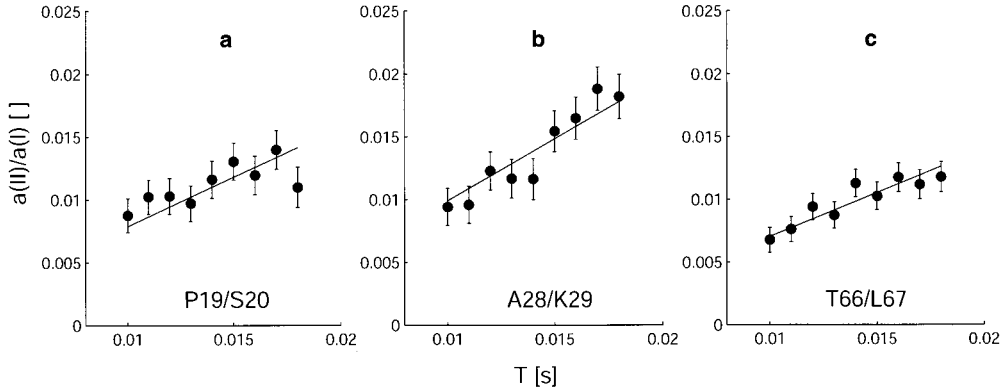

Figure 5. Typical build-up plots of the intensity ratios a(II)/a(I) observed as a function of the relaxation interval *T*. (a) The amino acid pair P19/S20 is located in a loop, (b) the pair A28/K29 is part of the α-1-helix, and (c) the pair T66/L67 is located in the *β*-4-sheet. The solid lines represent fits of experimental data to eq 2 using the Levenberg−Marquardt algorithm. The errors have been calculated by using error propagation with separate estimates of the noise in the spectra.

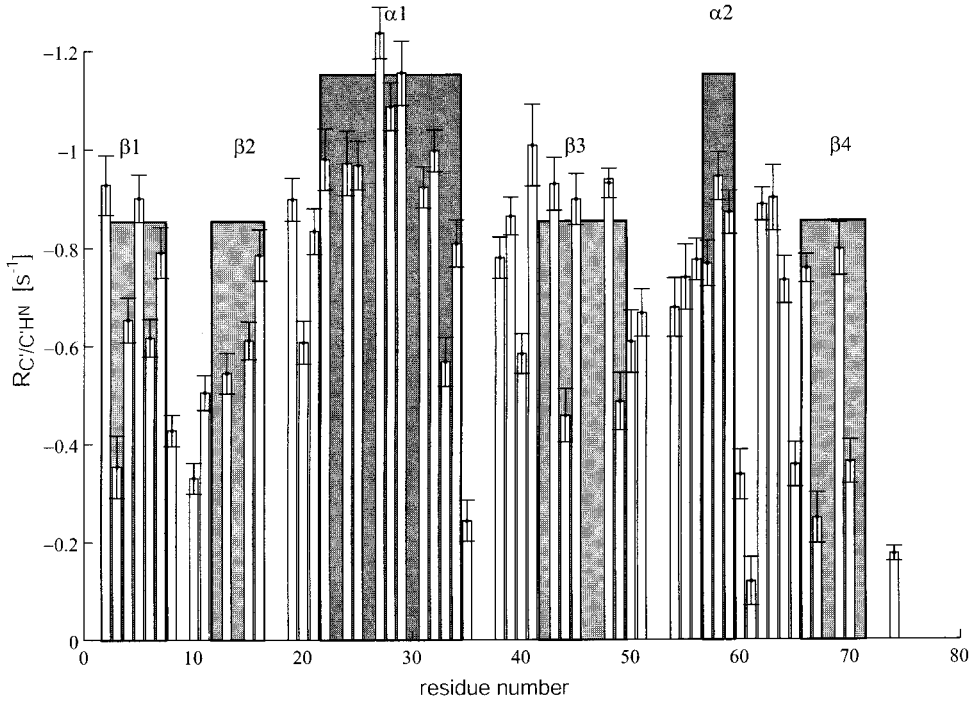

Figure 6. Cross-correlation rates $R_{C'/C'H^N}$ determined by the hybrid scheme of Figure 2. The white bars correspond to experimentally measured rates. Errors have been estimated by means of a Monte Carlo procedure. The shaded areas represent *β* sheets and α helices as discussed in the text.

time τ_e.[30] $P_2(x) = (3x^2 - 1)/2$ is the second-order Legendre polynomial. The cross-correlation order parameters $S^2_{ii,C'H^N}$ describe motional averaging of the correlation between the principal value σ_{ii} of the CSA tensor and the dipolar C′H^N interaction. If internal motions can be neglected, $S^2_{ii,C'H^N} = P_2(\cos\,\theta_{ii,C'H^N})$, where $\theta_{ii,C'H^N}$ are the angles between the σ_{ii} components and the CH vector ($\theta_{xx,C'H^N} = \alpha + 25°$ and $\theta_{yy,C'H^N} = \alpha + 115°$, see Figure 1).

Finally, Figure 6 displays the measured long-distance cross-correlation rates $R_{C'/C'H^N}$ corrected according to eq 4 with $\epsilon = 0.1$. The average is $\langle R_{C'/C'H^N}\rangle = -0.66 \pm 0.03\ s^{-1}$. In α helices, the mean rate is $\langle R_{C'/C'H^N}\rangle_\alpha = -0.95 \pm 0.03\ s^{-1}$, while the mean rate for *β* sheets is $\langle R_{C'/C'H^N}\rangle_\beta = -0.65 \pm 0.03\ s^{-1}$. The relative errors vary from about 5% to 40%. If one assumes that the C′ tensors are identical for all amino acids in ubiquitin, and if one uses average CSA tensor parameters obtained from bicellar solutions (mean parameters of Figure 1, $\alpha = 38°$, $\sigma_{xx} = -74.7$ ppm, $\sigma_{yy} = -11.8$ ppm, and $\sigma_{zz} = 86.5$ ppm, with respect to the isotropic shift),[31] one would expect the same rate $R_{C'/C'H^N} = -0.93\ s^{-1}$ for all residues. If one uses an average CSA tensor derived from solid-state NMR measurements ($\alpha = 35.7°$, $\sigma_{xx} = -73.6$ ppm, $\sigma_{yy} = -4$ ppm, and $\sigma_{zz} = 77.6$ ppm),[32] the expected rate would be $R_{C'/C'H^N} = -0.77\ s^{-1}$ for all residues. More refined estimates can be obtained if one assumes that the CSA tensors of all residues in α helices are the same, as could be determined for ubiquitin in bicellar solutions ($\alpha = 42°$, $\sigma_{xx} = -71.2$ ppm, $\sigma_{yy} = -23.3$ ppm, and $\sigma_{zz} = 94.5$ ppm),[31] and that all tensors in *β* sheets have common features ($\alpha = 37°$, $\sigma_{xx} = -76.5$ ppm, $\sigma_{yy} = -7.5$ ppm, and $\sigma_{zz} = 84$ ppm).[31] In Figure 6, the heights of the gray areas represent the rates expected for *β* strands and α helices in ubiquitin with $\tau_c = 4.1$ ns[28] *if internal*

(30) Lipari, G.; Szabo, A. *J. Am. Chem. Soc.* **1982**, *104*, 4546−4559.

(31) Bax, A.; Cornilescu, G. *J. Am. Chem. Soc.* **2000**, *122*, 10143−10154.

(32) Teng, Q.; Iqbal, M.; Cross, T. A. *J. Am. Chem. Soc.* **1992**, *114*, 5312−5321.

motions could be neglected. The ratio of the mean experimental rates in α helices and β strands, $\langle R_{C'/C'H^N}\rangle_\alpha/\langle R_{C'/C'H^N}\rangle_\beta = 0.7$, is the same as would be expected for CSA tensors determined in bicellar solutions.[31] This is likely to reflect changes in orientations and magnitudes of the CSA tensor components when comparing α helices and β strands. Besides differences between α helices and β strands, one notes large variations of the rates within any given region. This highlights the sensitivity of the cross-correlation rates $R_{C'/C'H^N}$ to local dynamics. Clearly, a quantitative determination of all parameters affecting $R_{C'/C'H^N}$ is impossible from a single measurement. To underline the complexity of the problem and to show the need for complementary rates, a qualitative discussion is presented below.

The distance $r_{C'H^N}$ determined by diffraction[33] varies between ca. 2.00 and 2.05 Å, which leads to a spread of 4% in $R_{C'/C'H^N}$. In the current analysis, we assume that the $N-H^N$ vector and the CSA tensor of the C′ atom are fixed with respect to the peptide plane. Slow conformational changes can only affect cross-correlations between these interactions if they modify the components of the C′ CSA tensor. Dramatic changes in the environment would be required to produce a significant modulation of the CSA components, which is unlikely to be caused by dynamic conformational changes, especially in structurally ordered regions of the protein. Even for the pair E24/N25, with a peptide plane that is subject to extensive slow motions,[34] the relaxation rate $R_{C'/C'H^N} = -0.92 \pm 0.04\ s^{-1}$ has a magnitude comparable to those found for other peptide planes in the same α-helical environment.

It is worth noting that the so-called *cross-correlated chemical shift modulations* (CSM/CSM)[12] of the isotropic shifts of the C′ and N nuclei, another manifestation of slow motions, are averaged out by the 180° pulse applied to the C′ carbons in the center of the MQC interval *T*.

Consequently, the large dispersion of the observed rates $R_{C'/C'H^N}$ in Figure 6 must result from "structural" variations of the CSA tensors from residue to residue and from the presence of *fast* internal motions (i.e., faster than the rotational diffusion of the molecule). That a variation of the *amplitudes* of the CSA components directly affects the magnitude of the rates $R_{C'/C'H^N}$ is easily seen from inspection of eq 5. A more detailed description of this effect has been presented by Zuiderweg and co-workers.[13] These variations can be due to changes in conformation[31,35] as they occur when going from α-helices to β-strands. Hydrogen bonds also influence the values of the C′ CSA tensors. In α-helices, σ_{yy} changes by about −14 ppm, while σ_{xx} increases by ca. +2 ppm upon formation of hydrogen bonds. In β-strands these components change by −10 and +4 ppm, respectively.[36] This would lead to an increase of $R_{C'/C'H^N}$ by about 25 and 20% in α-helices and β-strands, respectively.

Other factors influencing these rates are the presence of fast internal motions and local variations of the CSA tensor *orientations*. Because the latter determine how sensitive cross-correlation rates are to the former, their effects must be considered simultaneously. An investigation of the influence of motions on $R_{C'/C'H^N}$ has been presented elsewhere.[11,13] MD

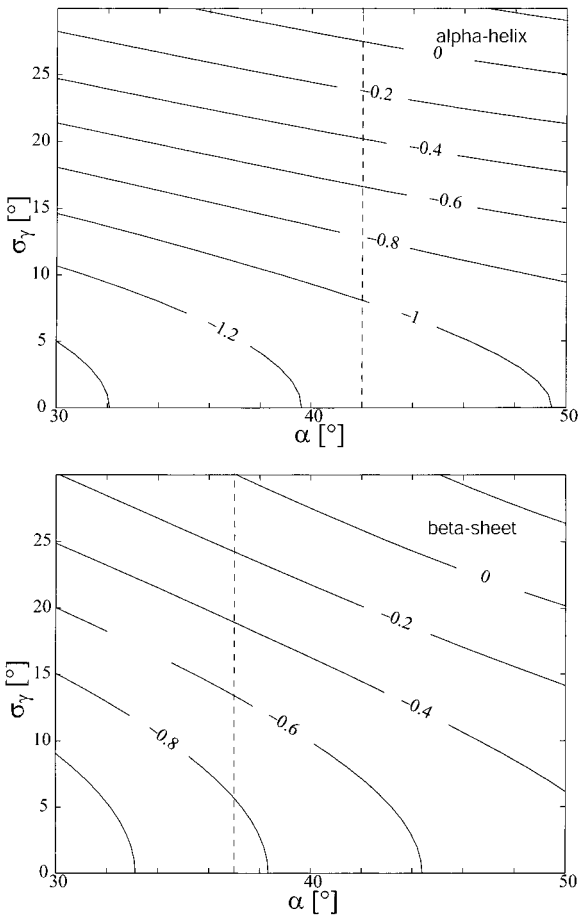

Figure 7. Contours indicating the predicted cross-correlation rate $R_{C'/C'H^N}$ as a function of CSA tensor orientations in the 1D GAF model. As shown in Figure 1, α is the angle between the CSA component σ_{xx} and the C′N bond, and σ_γ is the amplitude of the motion around the axis γ subtended by two consecutive C^α carbons. The rates are calculated for CSA tensors typical for α helices (top) and for β sheets (below). The vertical dashed lines indicate the mean α angles subtended between σ_{xx} and C′N that are typical for α helices and β sheets. In ubiquitin, amplitudes up to $\sigma_\gamma = 16$ or 20° have been reported in the literature,[34] which can account for almost all of the observed rates in Figure 6.

simulations have shown that significant motions[34] occur in structurally ordered regions of ubiquitin around an axis γ defined by the two C^α atoms in the peptide plane, as defined in Figure 1. In an attempt to describe their influence qualitatively, the order parameters in eq 6 may be calculated by using a 1D-GAF model[37] modified for the interference effect under investigation:

$$S^2_{ii,C'H^N} = P_2(\cos\theta_{ii,C'H^N}) - 3\sin\theta_{ii,\gamma}\times \sin\theta_{C'H^N,\gamma}\left\{-\cos\theta_{ii,\gamma}\cos\theta_{C'H^N,\gamma}(1-e^{-\sigma_\gamma{}^2}) + \frac{1}{4}\sin\theta_{ii,\gamma}\sin\theta_{C'H^N,\gamma}(1-e^{-4\sigma_\gamma{}^2})\right\} \quad (7)$$

where $\theta_{ii,\gamma}$ are the angles between the CSA tensor components σ_{ii} and the γ axis, $\theta_{C'H^N,\gamma}$ is the angle between the $C'H^N$ vector and γ, and $\theta_{ii,C'H^N}$ is the angle between σ_{ii} and the $C'H^N$ vector. Note that since all interactions lie in the same plane, no azimuthal dependence appears in eq 7. This expression can be derived either from the 1D-GAF model for auto-correlated

(33) Ramage, R.; Green, J.; Muir, T. W.; Ogunjobi, O. M.; Love, S.; Shaw, K. *Biochem. J.* **1994**, *299*, 151−158.
(34) Lienin, S. F.; Bremi, T.; Brutscher, B.; Brüschweiler, R.; Ernst, R. R. *J. Am. Chem. Soc.* **1998**, *120*, 9870−9879.
(35) Case, D. A. *Curr. Opin. Struct. Biol.* **2000**, *10*, 197−203.
(36) Walling, A. E.; Pargas, R. E.; de Dios, A. C. *J. Phys. Chem.* **1997**, *101*, 7299−7303.
(37) Brüschweiler, R.; Wright, P. E. *J. Am. Chem. Soc.* **1994**, *116*, 8426−8427.

relaxation or from a reduction of the 3D-GAF model,[38] where both interactions are assumed to be rigidly tied to the peptide plane and therefore experience motions of the same amplitude σ_γ. To account for possible structural variations of the CSA tensors, the order parameter S^2 was calculated for different angles α between σ_{xx} and C′N (see Figure 1) ranging from 30° to 50°. Figure 7a shows the expected variation in rates for a CSA tensor typical of an α helix, and Figure 7b shows the expected variation in rates for a tensor in a β sheet. To explain the dispersion of the $R_{C'/C'H^N}$ rates of Figure 6 by a static model would obviously require drastic changes in conformation. Clearly, only dynamic effects can explain the tremendous dispersion of the observed rates. Amplitudes of ca. 12−15° account for much of the attenuation of the rates with respect to those expected for a rigid molecule. Recent studies[39] suggest that some residues in ubiquitin exhibit motions of significant amplitudes around axes that are orthogonal to the γ axis. Moreover, structural variations of the angle α (see Figure 1) also have some influence on the $R_{C'/C'H^N}$ rates. Furthermore, the σ_{zz} component of the C′ tensor may not be perfectly perpendicular to the peptide plane, as it has been assumed so far, and the NH vector may also tip away from this plane. Consequently, a complete analysis of these parameters would require the measurement of several complementary cross-correlation rates.[6,39]

Conclusions

The approach described in this paper allows one to measure long-range cross-correlation rates in cases where the secular approximation would be violated if one used conventional single-quantum NMR. In addition, it is possible to separate two different cross-correlation mechanisms that have the same signature for multiple-quantum coherence by canceling the effects of the unwanted mechanism during a single-quantum interval. The method is no more time-consuming than conventional double-quantum spectroscopy and turns out to be remarkably insensitive to second-order effects. It can be applied to measure a wide variety of cross-correlation effects in systems that have small scalar couplings, the only condition being that one should be able to excite higher-order coherences that overcome the violation of the secular approximation. For example, in proteins it can be used to measure long-range cross-correlation effects $R_{C'/C'H^\alpha}$, $R_{C'H^N/C'H^\alpha}$, R_{N/NH^α}, $R_{C'C^\alpha/C'H^N}$, etc. In ubiquitin, under the conditions discussed above, these rates can be as large as 4, 1.5, 0.3, and 0.3 s^{-1}, that is, comparable to the rates $R_{C'/C'H^N}$ determined in this paper, which are on the order of 1 s^{-1}. The hybrid experiment can also be applied to nucleic acids with base pairs that are held together by hydrogen bonds between donor and acceptor nitrogen atoms $N^D-H\cdots N^A$.[9] It should be possible to measure cross-correlations N^A/HN^A between the fluctuations of the CSA tensor of the acceptor nitrogen N^A and the dipolar interaction $H\cdots N^A$. The procedure can be extended to coherences of arbitrary order. For example, if there is a violation of the secular approximation in the relaxation of double-quantum coherence, this may be resolved by resorting to an interval where triple-quantum coherence is allowed to evolve. The $R_{C'/C'H^N}$ cross-correlation rates measured in ubiquitin are very sensitive to fast local motions and appear very suitable for investigating protein dynamics.[11,13] "Structural" variations of the CSA tensors (i.e., local variations of magnitudes and orientations of their principal components) determine how sensitive the cross-correlation rates are to internal motions. This underscores the need to determine a number of complementary cross-correlation rates. The new method extends the number of cross-correlation rates that can be measured and therefore represents a significant step for the characterization of dynamics in biomolecules.

Acknowledgment. We thank Dr. Joel R. Tolman and Dr. Catherine Zwahlen for helpful comments and stimulating discussions. This work was supported by the Fonds National de la Recherche Scientifique and the Commission pour la Technologie et l'Innovation of Switzerland, and by the Centre National de la Recherche Scientifique of France.

Supporting Information Available: Three figures describing perturbations due to higher order effects and one figure showing the reproducibility of the experiment (PDF). This material is available free of charge via the Internet at http://pubs.acs.org.

JA011790V

(38) Bremi, T.; Brüschweiler, R. *J. Am. Chem. Soc.* **1997**, *119*, 6672−6673.
(39) Carlomagno, T.; Maurer, M.; Hennig, M.; Griesinger, C. *J. Am. Chem. Soc.* **2000**, *122*, 5105−5113.
(40) Levitt, M. H. *Prog. Nucl. Magn. Reson. Spectrosc.* **1986**, *18*, 61−122.
(41) Shaka, A. J.; Keeler, J.; Frenkiel, T.; Freeman, R. *J. Magn. Reson.* **1983**, *52*, 335.